Vision-Aided Complementary Filters for Attitude and Position Estimation of UAVs

João Pedro Dias Madeiras
joao.madeiras@tecnico.ulisboa.pt

Instituto Superior Técnico, Universidade de Lisboa, Lisbon, Portugal
June 2019

Abstract: This thesis presents two navigation systems based on Kalman complementary filtering for position and attitude estimation, with an application to Unmanned Air Vehicles (UAVs), in denied Global Positioning System (GPS) areas. Resorting to inertial measurements, vector observations and landmarks positioning, the proposed complementary filters provide attitude estimates resorting to Euler angles representation and position estimates relative to a fixed inertial frame. Both architectures share the same attitude filter, which estimates the Euler angles and rate gyro bias by exploiting a gyroscope noise model. In the first architecture, position and body velocity bias are estimated. The second architecture provides estimates on position, body velocities and acceleration bias. Stability and performance properties for the operating conditions are derived by Lyapunov theory and the procedure tuning of the filters' parameters in the frequency domain is detailed. Requirements on low computational burden were a priority in both the navigation system and especially in the vision algorithm, making it suitable for off-the-shelf hardware. Experimental results obtained in real time with an implementation of the proposed solutions with an AR.Drone 2.0 using two different built-in Simulink platforms are presented and discussed. The computation is provided by a laptop connected with the UAV in real time for the first approach. In the second, the proposed architectures run in real time fully onboard of the vehicle's processor.

Keywords: Navigation Systems, Complementary Kalman Filters, UAV, Stability, Lyapunov, Vision sensors

1. INTRODUCTION

Nowadays, the technological development and interest in low-cost UAVs have been on the rise in both civilian and military aviation sectors to accomplish different missions such as coastal surveillance operations, rescue, monitoring, security and inspection (Mohamed et al. (2018)).

In regular UAVs, Micro Electro Mechanical Systems (MEMS) are employed, which are low-cost and low-power consumption sensors, for the Inertial Navigation Systems (INS). Compared with high-end sensors like active ring-laser and interferometric fiber-optic sensor (P. Crain et al. (2010)), MEMS suffer from strong non-linearities such as bias and noise that degrade the accuracy of the estimates. To improve the performance and robustness of MEMS based INS, sensor fusion with an appropriate model are required to achieve a better attitude and position estimation and tracking. For this reason, current INSs rely on GPS signals to compensate position drift. To achieve optimal results with proved stability, Kalman filters (KFs) are the workhorse to fuse inertial measurement unit (IMU) and GPS measurements. One of the main limitations of the GPS-aided INS configuration is environments such as indoors, underground, underwater, in space, etc. In some cases, Visual-Aided INS can provide precise state estimates replacing the GPS.

This work focuses on the development of a Visual-Aided landmark positioning system aided IMU using complementary filters onboard of an Ar Drone 2.0. An innovative method is proposed by using color feature recognition for landmark tracking to compute position and attitude relative to a target via the algebraic Robust $O(n)$ solution to the Perspective-n-Point (RPnP) from Li et al. (2012). The obtained measurements are fused with the MEMS sensor outputs and with the Optical Flow (OF) velocity from the UAV. The problem of accurate position and attitude is addressed by exploiting the different range of relevant frequency regions presented in each measurement. The filtering solution is able to estimate accurately position, attitude.

The choice of type of filter technique in INS ranges from classical methodologies to recently proposed approaches. In the classical approach, KF is applied in real-time applications to fuse data from different sensors in an optimal way. The idea is to get independent and redundant information about navigation states, like position, attitude and velocity, and fuse them, with the requisite of having a prior information about the covariance values of both INS and position sensor as well statistical properties of each sensor system, see Gelb (1974). Extended Kalman Filter (EKF) is a nonlinear filtering technique where a nonlinear model is considered and a linearization occurs each time to get Kalman gains. However, the linearization implicit in EKF leads to performance degradation or even filter divergence if the assumption of local linearity is violated (Maybeck (1994)). In Crassidis et al. (2007) and Mahony et al. (2008), a number of other alternative techniques are introduced, namely Unscented Kalman Filters (UKF), Particle Filters (PF), Adaptive Methods and Nonlinear Observers.

The INS in this work is designed to be easily implemented in a low-cost, low-power consumption hardware architecture. Therefore, high computation cost filters like EKF, UKF and PF were out of the equation. The complementary Kalman filters proposed in this work are time-varying, although the gains are computed offline using an auxiliary time-invariant design system that by means of a Lyapunov transformation becomes the proposed filter (Vasconcelos et al. (2011)). The main contribution of this thesis is the

INS performance validation onboard of an AR.Drone 2.0 in real time.

This extended abstract is organized as follows. Section 2 presents the deduction of the complementary filters and their stability and performance properties are discussed. Section 3 shows the implementation of the INS using both attitude and position filters combined. Filter observations based on IMU and vision sensors are discussed. In Section 4 the INS experimental results onboard of an Ar Drone 2.0 are shown and its performance analyzed. Concluding remarks are pointed out in Section 5.

2. ATTITUDE AND POSITION COMPLEMENTARY FILTERS

In this section, complementary filters for attitude and position are proposed and their performance and stability is proven. The attitude filter is design making use of Alan Variance angular velocity to model its noise and a vector of measurements computed from accelerometer data. The position filter is designed in the frequency domain using the OF's velocity as input and position measurement from a landmark.

2.1 Attitude Filter

Gyroscope Noise Model. According to Ünver (2013), the most predominant noises in a MEMS gyroscope are the angle random walk (ARW), bias instability (BI) and rate random walk (RRW). For more information about gyro's noises and how they can be modelled, please refer to Petkov and Slavov (2010).

ARW is a high-frequency noise modelled as a zero-mean white noise with an approximated variance:

$$\sigma_{arw}^2 = \frac{N^2}{\Delta t} \tag{1}$$

where Δt is the sampling time interval and N is the ARW parameter from the Allan Deviation (AD) plot.

BI has an impact on long term stability and can be approximated by a Markov process (Petkov and Slavov (2010)), with a process standard deviation proportional to the AD parameter B. The discrete time of $b_{\omega 1}$ at time k subject to the sample-and-hold method is given by:

$$b_{\omega 1 k+1} = \left(1 - \frac{1}{T}\Delta t\right) b_{\omega 1 k} + v_k \tag{2}$$

where k the index of time $t = k\Delta t$, $b_{\omega 1}$ is a random process, T corresponds to the correlation time of BI and v_k a driven zero-mean white noise with variance ${\sigma_v}^2 = \sigma_b^2\left(1 - e^{-2\Delta t/T}\right)$, where $\sigma_b^2 = \frac{2B^2}{\pi}\ln(2)$ is the variance of BI. T can be obtained from AD plot around the BI region.

RRW occurs whenever a zero-mean white noise is integrated over time. The discrete time of $b_{\omega 2}$ at time k subject to sample-and-hold method, is given by:

$$b_{\omega 2 k+1} = b_{\omega 2 k} + \eta_k \tag{3}$$

where η_k is a zero-mean white noise with variance ${\sigma_\eta}^2 = \Delta t K^2$, K is the RRW parameter from AD plot.

In line with the previously described noises formulations, the gyro noise model is given in discrete state-space form as Quinchia et al. (2013):

$$\begin{aligned} \boldsymbol{b}_{\boldsymbol{\omega} k+1} &= \begin{bmatrix} \left(1 - \frac{1}{T}\Delta t\right) & 0 \\ 0 & 1 \end{bmatrix} \begin{bmatrix} b_{\omega 1} \\ b_{\omega 2} \end{bmatrix}_k \\ &+ \begin{bmatrix} \sqrt{\sigma_b^2\left(1 - e^{-2\Delta t/T}\right)} \\ \sqrt{K^2 \Delta t} \end{bmatrix} \boldsymbol{w}_k \\ y_k &= [1 \ \ 1] \begin{bmatrix} b_{\omega 1} \\ b_{\omega 2} \end{bmatrix}_k + \left[\sqrt{\frac{N^2}{\Delta t}} \right] \zeta_k \end{aligned} \tag{4}$$

where $\boldsymbol{w}_k$ and ζ_k are normally distributed zero-mean white noises.

Filter. Let $\boldsymbol{\lambda} = [\psi \ \theta \ \phi]^T$ be the vector containing the true Euler angles yaw, pitch and roll, respectively. Euler angles kinematic is given by:

$$\dot{\boldsymbol{\lambda}} = \boldsymbol{Q}(\boldsymbol{\lambda})\boldsymbol{\omega}, \quad \boldsymbol{Q}(\boldsymbol{\lambda}) = \begin{bmatrix} 0 & \sin(\phi)\sec(\theta) & \cos(\phi)\sec(\theta) \\ 0 & \cos(\phi) & -\sin(\phi) \\ 1 & \sin(\phi)\tan(\theta) & \cos(\phi)\tan(\theta) \end{bmatrix} \tag{5}$$

where $\boldsymbol{\omega} = [\omega_x \ \omega_y \ \omega_z]^T$ is the true angular velocity in the body frame. The discrete-time equivalent system of (5), resorting to the step invariant method, is:

$$\boldsymbol{\lambda}_{k+1} = \boldsymbol{\lambda}_k + \Delta t \boldsymbol{Q}(\boldsymbol{\lambda}_k)\boldsymbol{\omega}_k \tag{6}$$

The angular velocity is measured by the gyroscope subjected to noise is given by:

$$\boldsymbol{\omega}_k = \bar{\boldsymbol{\omega}}_k + \boldsymbol{y}_k \tag{7}$$

where $\bar{\boldsymbol{\omega}}_{\boldsymbol{k}}$ represents the value of angular velocities and $\boldsymbol{y}_k$ the output of the noise model (4) for each velocity. Rewriting the kinematic of Euler angles (6-7) in state space form yields:

$$\begin{aligned} &\begin{bmatrix} \boldsymbol{\lambda} \\ \boldsymbol{b_{\omega 1}} \\ \boldsymbol{b_{\omega 2}} \end{bmatrix}_{k+1} = \begin{bmatrix} \boldsymbol{I} & -\Delta t \boldsymbol{Q}(\boldsymbol{\lambda}_k) & -\Delta t \boldsymbol{Q}(\boldsymbol{\lambda}_k) \\ \boldsymbol{0} & \boldsymbol{I} - \Delta t \boldsymbol{T}^{-1} & \boldsymbol{0} \\ \boldsymbol{0} & \boldsymbol{0} & \boldsymbol{I} \end{bmatrix} \begin{bmatrix} \boldsymbol{\lambda} \\ \boldsymbol{b_{\omega 1}} \\ \boldsymbol{b_{\omega 2}} \end{bmatrix}_k + \\ &\begin{bmatrix} \Delta t \boldsymbol{Q}(\boldsymbol{\lambda}_k) \\ \boldsymbol{0} \\ \boldsymbol{0} \end{bmatrix} \boldsymbol{\omega_k} + \begin{bmatrix} -\Delta t \boldsymbol{Q}(\boldsymbol{\lambda}_k) & \boldsymbol{0} & \boldsymbol{0} \\ \boldsymbol{0} & \boldsymbol{I} & \boldsymbol{0} \\ \boldsymbol{0} & \boldsymbol{0} & \boldsymbol{I} \end{bmatrix} \begin{bmatrix} \boldsymbol{n_{arw}} \\ \boldsymbol{n_{bi}} \\ \boldsymbol{n_{rrw}} \end{bmatrix} \\ &\boldsymbol{y_{\lambda}}_k = \begin{bmatrix} \boldsymbol{I} & \boldsymbol{0} & \boldsymbol{0} \end{bmatrix} \begin{bmatrix} \boldsymbol{\lambda} \\ \boldsymbol{b_{\omega 1}} \\ \boldsymbol{b_{\omega 2}} \end{bmatrix}_k + \boldsymbol{\Theta}_k \end{aligned} \tag{8}$$

where $\boldsymbol{b_{\omega 1}}$ and $\boldsymbol{b_{\omega 2}}$ are sensor bias vectors correspondent to the angular velocities $\boldsymbol{\omega}$. Considering the following nonlinear feedback system of (8), as the proposed attitude filter, depicted in Fig. 1:

$$\begin{aligned} &\begin{bmatrix} \hat{\boldsymbol{\lambda}} \\ \hat{\boldsymbol{b}}_{\boldsymbol{\omega 1}} \\ \hat{\boldsymbol{b}}_{\boldsymbol{\omega 2}} \end{bmatrix}_{k+1} = \begin{bmatrix} \boldsymbol{I} & -\Delta t \boldsymbol{Q}(\boldsymbol{\lambda}_k) & -\Delta t \boldsymbol{Q}(\boldsymbol{\lambda}_k) \\ \boldsymbol{0} & \boldsymbol{I} - \Delta t \boldsymbol{T}^{-1} & \boldsymbol{0} \\ \boldsymbol{0} & \boldsymbol{0} & \boldsymbol{I} \end{bmatrix} \begin{bmatrix} \hat{\boldsymbol{\lambda}} \\ \hat{\boldsymbol{b}}_{\boldsymbol{\omega 1}} \\ \hat{\boldsymbol{b}}_{\boldsymbol{\omega 2}} \end{bmatrix}_k + \begin{bmatrix} \Delta t \boldsymbol{Q}(\boldsymbol{\lambda}_k) \\ \boldsymbol{0} \\ \boldsymbol{0} \end{bmatrix} \boldsymbol{\omega_k} \\ &+ \begin{bmatrix} \boldsymbol{Q}(\boldsymbol{\lambda}_k)(\boldsymbol{K_{1\lambda}} - \boldsymbol{I}) + \boldsymbol{Q}(\boldsymbol{\lambda}_{k-1}) \\ \boldsymbol{K_{2\lambda}} \\ \boldsymbol{K_{3\lambda}} \end{bmatrix} \boldsymbol{Q^{-1}}(\boldsymbol{\lambda}_{k-1})(\boldsymbol{\lambda}_k - \hat{\boldsymbol{\lambda}}_k) \end{aligned} \tag{9}$$

where the hat means estimate, $\boldsymbol{\lambda}_k$ is the observed Euler angles corrupted by a Gaussian zero-mean white-noise $\boldsymbol{\Theta}_k$, and $\boldsymbol{K_{1\lambda}}$, $\boldsymbol{K_{2\lambda}}$, $\boldsymbol{K_{3\lambda}} \in$ M(3,3) are feedback gain matrices. The attitude observation $\boldsymbol{\lambda}_k$ can be obtained by measuring the Earth's gravitational and magnetic fields or by other observations such as cameras. Rewriting the attitude kinematics (8) considering $\boldsymbol{I}$ in place of $\boldsymbol{Q}(\boldsymbol{\lambda})$ and $\boldsymbol{\omega_k} = \boldsymbol{0}$ results in a linear time invariant system:

$$\begin{bmatrix} \boldsymbol{X_\lambda} \\ \boldsymbol{X_{b_{\omega 1}}} \\ \boldsymbol{X_{b_{\omega 2}}} \end{bmatrix}_{k+1} = \begin{bmatrix} \boldsymbol{I} & -\Delta t\boldsymbol{I} & -\Delta t\boldsymbol{I} \\ \boldsymbol{0} & \boldsymbol{I}-\Delta t\boldsymbol{T}^{-1} & \boldsymbol{0} \\ \boldsymbol{0} & \boldsymbol{0} & \boldsymbol{I} \end{bmatrix} \begin{bmatrix} \boldsymbol{X_\lambda} \\ \boldsymbol{X_{b_{\omega 1}}} \\ \boldsymbol{X_{b_{\omega 2}}} \end{bmatrix}_{k} + \begin{bmatrix} -\Delta t\boldsymbol{I} & \boldsymbol{0} & \boldsymbol{0} \\ \boldsymbol{0} & \boldsymbol{I} & \boldsymbol{0} \\ \boldsymbol{0} & \boldsymbol{0} & \boldsymbol{I} \end{bmatrix} \begin{bmatrix} \boldsymbol{n_{arw}} \\ \boldsymbol{n_{bi}} \\ \boldsymbol{n_{rrw}} \end{bmatrix}_k$$
$$\boldsymbol{y}_{X\,k} = \begin{bmatrix} \boldsymbol{I} & \boldsymbol{0} & \boldsymbol{0} \end{bmatrix} \begin{bmatrix} \boldsymbol{X_\lambda} \\ \boldsymbol{X_{b_{\omega 1}}} \\ \boldsymbol{X_{b_{\omega 2}}} \end{bmatrix}_{k} + \boldsymbol{\Theta}_k \tag{10}$$

Can be proven, Asymptotic stability of the system (9) with $\boldsymbol{K_{1\lambda}}$, $\boldsymbol{K_{2\lambda}}$ and $\boldsymbol{K_{3\lambda}}$ being the steady state Kalman gains of (10), if the pitch angle is bounded, $|\theta| < \theta_{max} < \frac{\pi}{2}$, by means of a Lyapunov transformation on the error's closed loop.

Theorem 1. Consider the discrete-time system (8). Let $\boldsymbol{K_{1\lambda}}$, $\boldsymbol{K_{2\lambda}}$ and $\boldsymbol{K_{3\lambda}}$ be the steady-state Kalman gains for the system (10) and assume a bounded pitch for the UAV, $|\theta| < \theta_{max} < \frac{\pi}{2}$. Then the attitude complementary filter (9) is uniformly asymptotically stable (UAS).

Proof. Let $\widetilde{\boldsymbol{\lambda}}_k = \boldsymbol{\lambda}_k - \hat{\boldsymbol{\lambda}}_k$, $\widetilde{\boldsymbol{b}}_{\boldsymbol{\omega i}_k} = \boldsymbol{b}_{\boldsymbol{\omega i}_k} - \hat{\boldsymbol{b}}_{\boldsymbol{\omega i}_k}$ denote the estimation errors. This error dynamics are given by

$$\begin{bmatrix} \widetilde{\boldsymbol{\lambda}} \\ \widetilde{\boldsymbol{b}}_{\boldsymbol{\omega 1}} \\ \widetilde{\boldsymbol{b}}_{\boldsymbol{\omega 2}} \end{bmatrix}_{k+1} = \begin{bmatrix} \boldsymbol{Q}(\boldsymbol{\lambda}_k)(\boldsymbol{I}-\boldsymbol{K_{1\lambda}})\boldsymbol{Q}^{-1}(\boldsymbol{\lambda}_{k-1}) & -\Delta t\boldsymbol{Q}(\boldsymbol{\lambda}_k) & -\Delta t\boldsymbol{Q}(\boldsymbol{\lambda}_k) \\ -\boldsymbol{K_{2\lambda}}\boldsymbol{Q}^{-1}(\boldsymbol{\lambda}_{k-1}) & \boldsymbol{I}-\Delta t\boldsymbol{T}^{-1} & \boldsymbol{0} \\ -\boldsymbol{K_{3\lambda}}\boldsymbol{Q}^{-1}(\boldsymbol{\lambda}_{k-1}) & \boldsymbol{0} & \boldsymbol{I} \end{bmatrix} \begin{bmatrix} \widetilde{\boldsymbol{\lambda}} \\ \widetilde{\boldsymbol{b}}_{\boldsymbol{\omega 1}} \\ \widetilde{\boldsymbol{b}}_{\boldsymbol{\omega 2}} \end{bmatrix}_{k} + \begin{bmatrix} -\Delta t\boldsymbol{Q}(\boldsymbol{\lambda}_k) & \boldsymbol{0} & \boldsymbol{0} \\ \boldsymbol{0} & \boldsymbol{I} & \boldsymbol{0} \\ \boldsymbol{0} & \boldsymbol{0} & \boldsymbol{I} \end{bmatrix} \boldsymbol{\omega}_k + \begin{bmatrix} \boldsymbol{Q}(\boldsymbol{\lambda}_k)(\boldsymbol{I}-\boldsymbol{K_{1\lambda}}) - \boldsymbol{Q}(\boldsymbol{\lambda}_{k-1}) \\ -\boldsymbol{K_{2\lambda}} \\ -\boldsymbol{K_{3\lambda}} \end{bmatrix} \boldsymbol{\Theta}_{\boldsymbol{\lambda}k} \tag{11}$$

By definition, the filter (11) is UAS if its origin is UAS in the absence of state and measurement noises, see Jazwinski (1970). Nonetheless, the state and measurement noises are explicit in the proof for convenience. The system (10) can be rewritten in a compact state space formulation:

$$\boldsymbol{X}_{k+1} = \boldsymbol{F}\boldsymbol{X}_k + \boldsymbol{G}\boldsymbol{n}_k,\ \boldsymbol{y}_{\boldsymbol{X}k} = \boldsymbol{H}\boldsymbol{X}_k + \boldsymbol{\Theta}_k \tag{12}$$

where $\boldsymbol{X}$, $\boldsymbol{n}_k$, $\boldsymbol{y}_{\boldsymbol{X}k}$, $\boldsymbol{F}$ and $\boldsymbol{G}$ are the vectors and matrices found in (10). It is straightforward to show that the observability and controllability matrices of system (10) are full rank, hence the close-loop system

$$\widetilde{\boldsymbol{X}}_{k+1} = (\boldsymbol{F} - \boldsymbol{K}\boldsymbol{H})\,\widetilde{\boldsymbol{X}}_k + \boldsymbol{G}\boldsymbol{n}_k - \boldsymbol{K}\boldsymbol{\Theta}_k \tag{13}$$

where $\boldsymbol{K} = \begin{bmatrix} \boldsymbol{K}_{1\lambda}' & \boldsymbol{K}_{2\lambda}' & \boldsymbol{K}_{3\lambda}' \end{bmatrix}^T$, is UAS (see Anderson and Moore (1979)). Define the Lyapunov transformation of variables:

$$\begin{bmatrix} \widetilde{\boldsymbol{\lambda}}_X \\ \widetilde{\boldsymbol{b}}_{\boldsymbol{\omega 1}\,X} \\ \widetilde{\boldsymbol{b}}_{\boldsymbol{\omega 2}\,X} \end{bmatrix}_k = \boldsymbol{T}_k \begin{bmatrix} \widetilde{\boldsymbol{X}}_\lambda \\ \widetilde{\boldsymbol{X}}_{b_{\omega 1}} \\ \widetilde{\boldsymbol{X}}_{b_{\omega 2}} \end{bmatrix}_k,\ \boldsymbol{T}_k = \begin{bmatrix} \boldsymbol{Q}(\boldsymbol{\lambda}_{k-1}) & \boldsymbol{0} & \boldsymbol{0} \\ \boldsymbol{0} & \boldsymbol{I} & \boldsymbol{0} \\ \boldsymbol{0} & \boldsymbol{0} & \boldsymbol{I} \end{bmatrix} \tag{14}$$

which according to Rugh (1996) is well defined with the assumption that θ is bounded. Applying the Lyapunov transformation $\boldsymbol{T}_k$ to (13) yields

$$\begin{bmatrix} \widetilde{\boldsymbol{\lambda}}_X \\ \widetilde{\boldsymbol{b}}_{\boldsymbol{\omega 1}\,X} \\ \widetilde{\boldsymbol{b}}_{\boldsymbol{\omega 2}\,X} \end{bmatrix}_{k+1} = \begin{bmatrix} \boldsymbol{Q}(\boldsymbol{\lambda}_k)(\boldsymbol{I}-\boldsymbol{K_{1\lambda}})\boldsymbol{Q}^{-1}(\boldsymbol{\lambda}_{k-1}) & -\Delta t\boldsymbol{Q}(\boldsymbol{\lambda}_k) & -\Delta t\boldsymbol{Q}(\boldsymbol{\lambda}_k) \\ -\boldsymbol{K_{2\lambda}}\boldsymbol{Q}^{-1}(\boldsymbol{\lambda}_{k-1}) & \boldsymbol{I}-\Delta t\boldsymbol{T}^{-1} & \boldsymbol{0} \\ -\boldsymbol{K_{3\lambda}}\boldsymbol{Q}^{-1}(\boldsymbol{\lambda}_{k-1}) & \boldsymbol{0} & \boldsymbol{I} \end{bmatrix} \begin{bmatrix} \widetilde{\boldsymbol{\lambda}}_X \\ \widetilde{\boldsymbol{b}}_{\boldsymbol{\omega 1}\,X} \\ \widetilde{\boldsymbol{b}}_{\boldsymbol{\omega 2}\,X} \end{bmatrix}_{k} + \begin{bmatrix} -\Delta t\boldsymbol{Q}(\boldsymbol{\lambda}_k) & \boldsymbol{0} & \boldsymbol{0} \\ \boldsymbol{0} & \boldsymbol{I} & \boldsymbol{0} \\ \boldsymbol{0} & \boldsymbol{0} & \boldsymbol{I} \end{bmatrix} \boldsymbol{\omega}_k + \begin{bmatrix} -\boldsymbol{Q}(\boldsymbol{\lambda}_k)\boldsymbol{K_{1\lambda}} \\ -\boldsymbol{K_{2\lambda}} \\ -\boldsymbol{K_{3\lambda}} \end{bmatrix} \boldsymbol{v}_{\lambda k} \tag{15}$$

The origin of (13) is UAS and, by the Lyapunov transformation properties, the origin of (15) as well. Therefore, the origin of (11) is uniformly asymptotically stable.

Considering slow maneuvers, the performance of the proposed attitude filter with the steady state Kalman gains of the system (10) is identical to that of a Kalman filter designed for the time-varying system (8).

Proposition 2. Let the state and observation disturbances in the attitude kinematics (8) be characterized by the zero-mean Gaussian white noises $\boldsymbol{n_{arw}}$, $\boldsymbol{n_{bi}}$, $\boldsymbol{n_{rrw}}$ and $\boldsymbol{v_k}$, respectively, and assume that pitch and roll angles are constant. Then the complementary filter (9) is the "steady state" Kalman filter for the system (8) in the sense that the Kalman feedback gain K_{optk} converges asymptotically as follows:

$$\lim_{k\to\infty} \left\| \boldsymbol{K_{opt}}_k - \begin{bmatrix} \boldsymbol{Q}(\boldsymbol{\lambda}_k)(\boldsymbol{K_{1\lambda}} - \boldsymbol{I}) + \boldsymbol{Q}(\boldsymbol{\lambda}_{k-1}) \\ \boldsymbol{K_{2\lambda}} \\ \boldsymbol{K_{3\lambda}} \end{bmatrix} \right\| = \boldsymbol{0} \tag{16}$$

Proof. An analogous proof can be found in theorem 2 of Vasconcelos et al. (2011).

This holds for small variations in pitch and roll. For aggressive maneuvers with a time-varying pitch and roll the filter's performance can be compared offline by computing the estimation error covariances of the filters as in Appendix A of Vasconcelos et al. (2011).

2.2 Position Filter with Velocity Bias

The proposed position filter is based on the complementary attitude filter proposed by Vasconcelos et al. (2011), where the Euler angles become the UAV inertial position $\boldsymbol{p}$, and the input, instead of being the angular velocity will be the UAV body frame's velocity ${}^B\boldsymbol{v}$.

The continuous-time position kinematics are given by:

$$\dot{\boldsymbol{p}} = \boldsymbol{v} \tag{17}$$

where $\boldsymbol{p}$ and $\boldsymbol{v}$ are the position and velocity in the chosen inertial frame coordinates. Let $\boldsymbol{R}^I$ be the rotational matrix from body frame $\{B\}$ to inertial frame $\{I\}$. The discrete-time equivalent subject to a sample-and-hold becomes:

$$\boldsymbol{p}_{k+1} = \boldsymbol{p}_k + \Delta t \boldsymbol{R}_k^I {}^B\boldsymbol{v}_k \tag{18}$$

The OF from bottom the camera measures the velocity relative to the ground on UAV body frame giving:

$${}^B\boldsymbol{v}_k = {}^B\bar{\boldsymbol{v}}_k + \boldsymbol{b}_{\boldsymbol{v}\,k} + \boldsymbol{n}_{bk} \tag{19}$$

where ${}^B\bar{\boldsymbol{v}}_k$ denote the true body velocity, $\boldsymbol{b}_{\boldsymbol{v}\,k}$ the velocity bias and $\boldsymbol{n}_{bk}$ a zero-mean white-noise.

The position kinematics (18), using the OF's measurements, are described in state-space form by:

$$\begin{bmatrix} \boldsymbol{p} \\ \boldsymbol{b_v} \end{bmatrix}_{k+1} = \begin{bmatrix} \boldsymbol{I} & -\Delta t\boldsymbol{R}_k^I \\ \boldsymbol{0} & \boldsymbol{I} \end{bmatrix} \begin{bmatrix} \boldsymbol{p} \\ \boldsymbol{b_v} \end{bmatrix}_k + \begin{bmatrix} \Delta t\boldsymbol{R}_k^I \\ \boldsymbol{0} \end{bmatrix} {}^B\boldsymbol{v}_k + \begin{bmatrix} -\Delta t\boldsymbol{R}_k^I & \boldsymbol{0} \\ \boldsymbol{0} & \boldsymbol{I} \end{bmatrix} \begin{bmatrix} \boldsymbol{n_p} \\ \boldsymbol{n_b} \end{bmatrix}_k \tag{20}$$

where $\boldsymbol{n}_{\boldsymbol{p}_k}$ is a zero-mean Gaussian white noise that accounts for disturbance in the position. The position observer, depicted in Fig. 1, is given by the following nonlinear feedback system:

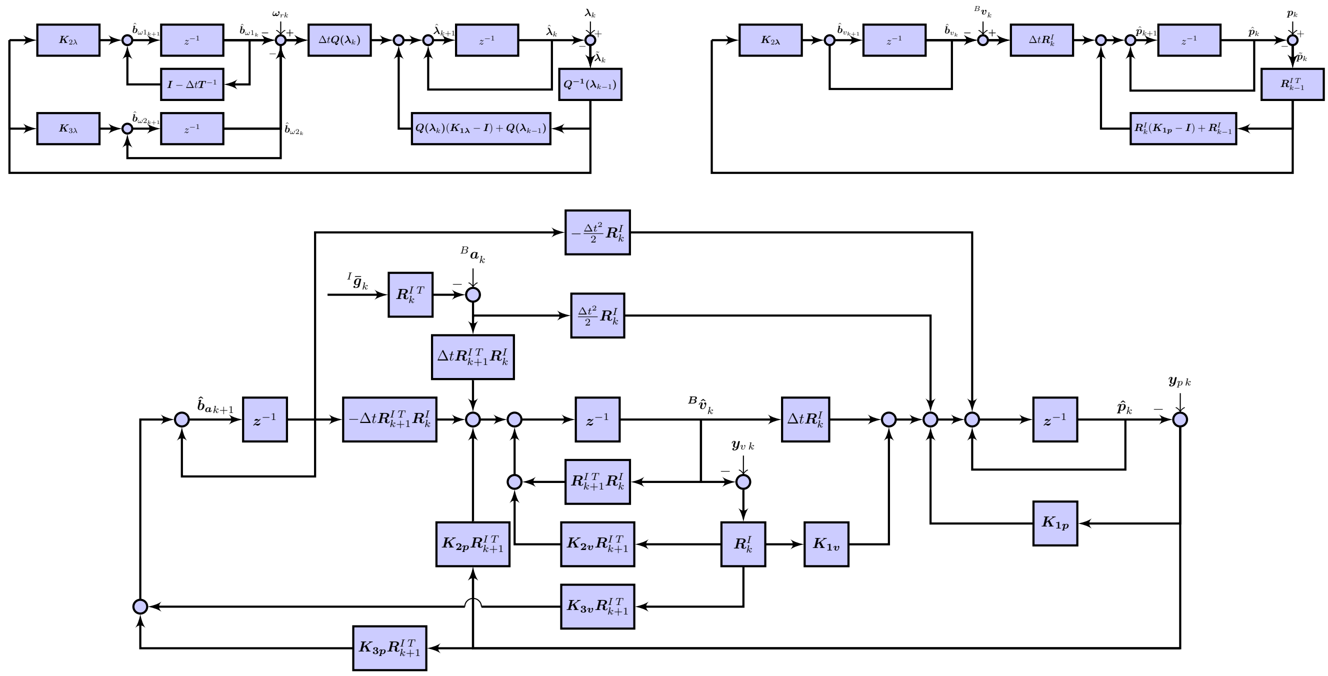

Fig. 1. Attitude (top left), position with velocity bias (top right) and position with acceleration bias (bottom) filter block diagrams.

$$\begin{bmatrix}\hat{\boldsymbol{p}}\\ \hat{\boldsymbol{b}}_{\boldsymbol{v}}\end{bmatrix}_{k+1} = \begin{bmatrix}\boldsymbol{I} & -\Delta t\boldsymbol{R}^I_k\\ \boldsymbol{0} & \boldsymbol{I}\end{bmatrix}\begin{bmatrix}\hat{\boldsymbol{p}}\\ \hat{\boldsymbol{b}}_{\boldsymbol{v}}\end{bmatrix}_k + \begin{bmatrix}\Delta t\boldsymbol{R}^I_k\\ \boldsymbol{0}\end{bmatrix}{}^B\boldsymbol{v}_k + \begin{bmatrix}\boldsymbol{R}^I_k(\boldsymbol{K_{1p}}-\boldsymbol{I})+\boldsymbol{R}^I_{k-1}\\ \boldsymbol{K_{2b_v}}\end{bmatrix}\boldsymbol{R}^{I\,T}_{k-1}(\boldsymbol{p}_k-\hat{\boldsymbol{p}}_k) \tag{21}$$

It is proved by Vasconcelos et al. (2011) that if $\boldsymbol{K_{1p}}$ and $\boldsymbol{K_{2b_v}}$ are the Kalman gains for the system (20) with $\boldsymbol{R}^I_k = \boldsymbol{I}$, with the small difference that here pitch does not have to be bounded, then the filter (21) is uniformly asymptotically stable (UAS). Another extended proof can be deduced from Vasconcelos et al. (2011) is that assuming zero-mean Gaussian noise for the state and observation disturbances, without the need of having roll and pitch constant, the complementary filter (21) is the "steady state" Kalman filter for the system (20) in the sense that the Kalman feedback gain $\boldsymbol{K_{opt\,k}}$ converges asymptotically as follows:

$$\lim_{k\to\infty}\left\|\boldsymbol{K_{opt\,k}} - \begin{bmatrix}\boldsymbol{R}^I_k(\boldsymbol{K_{1p}}-\boldsymbol{I})+\boldsymbol{R}^I_{k-1}\\ \boldsymbol{K_{2b}}\end{bmatrix}\right\| = \boldsymbol{0} \tag{22}$$

2.3 Position Filter with acceleration bias

The proposed position filter goes further than the previous subsection by considering the acceleration in the dynamic model. Position, velocity and acceleration bias are considered as state variables.

The continuous-time position and velocity kinematics are given by:

$$\begin{cases}\dot{\boldsymbol{v}} = \boldsymbol{a}\\ \dot{\boldsymbol{p}} = \boldsymbol{v}\end{cases} \tag{23}$$

where $\boldsymbol{p}$, $\boldsymbol{v}$ and $\boldsymbol{a}$ are the position, velocity and linear acceleration in a chosen inertial frame coordinates, respectively. Let $\boldsymbol{R}^I$ be the rotational matrix from body frame $\{B\}$ to inertial frame $\{I\}$. The discrete-time equivalent subject to a sample-and-hold can be given by (Vasconcelos et al. (2011)):

$$\begin{cases}\boldsymbol{p}_{k+1} = \boldsymbol{p}_k + \Delta t\boldsymbol{R}^I_k{}^{\boldsymbol{B}}\boldsymbol{v}_k + \dfrac{\Delta t^2}{2}\boldsymbol{R}^I_k{}^B\boldsymbol{a}_k\\ {}^{\boldsymbol{B}}\boldsymbol{v}_{k+1} = \boldsymbol{R}^{I\,T}_{k+1}\boldsymbol{R}^I_k{}^{\boldsymbol{B}}\boldsymbol{v}_k + \Delta t\boldsymbol{R}^{I\,T}_{k+1}\boldsymbol{R}^I_k{}^B\boldsymbol{a}_k\\ \boldsymbol{v}_k = \boldsymbol{R}^I_k{}^{\boldsymbol{B}}\boldsymbol{v}_k\\ \boldsymbol{a}_k = \boldsymbol{R}^I_k{}^B\boldsymbol{a}_k\end{cases} \tag{24}$$

where ${}^{\boldsymbol{B}}\boldsymbol{v}_k$ and ${}^B\bar{\boldsymbol{a}}_k$ are the velocity and acceleration in the body frame, respectively.

The accelerometer measures the specific force, which is the difference between the inertial and the gravitational acceleration of the rigid body, and is modelled in the body frame $\{B\}$ as:

$${}^{\boldsymbol{B}}\boldsymbol{a}_k = {}^B\bar{\boldsymbol{a}}_k - {}^B\bar{\boldsymbol{g}}_k + \boldsymbol{b}_{\boldsymbol{a}\,k} + \boldsymbol{n}_{\boldsymbol{a}\,k} \tag{25}$$

where ${}^B\bar{\boldsymbol{a}}_k$ denote the true body acceleration, ${}^B\bar{\boldsymbol{g}}_k$ the true gravitational acceleration, $\boldsymbol{n}_{\boldsymbol{a}\,k}$ a zero-mean white-noise and $\boldsymbol{b}_{\boldsymbol{a}\,k}$ a fast driving bias term that accounts for non-modeled behavior, e.g. centripetal acceleration, modeled as:

$$\boldsymbol{b}_{\boldsymbol{a}\,k+1} = \boldsymbol{R}^{I\,T}_{k+1}\boldsymbol{R}^I_k\left(\boldsymbol{b}_{\boldsymbol{a}\,k} + \boldsymbol{n}_{\boldsymbol{b_a}\,k}\right) \tag{26}$$

where $\boldsymbol{n}_{\boldsymbol{b_a}}$ is a zero-mean white-noise.

The position kinematics (24), using the accelerometer model (25-26), are described in state-space form by:

$$\begin{bmatrix} \boldsymbol{p} \\ {}^B\boldsymbol{v} \\ \boldsymbol{b_a} \end{bmatrix}_{k+1} = \begin{bmatrix} \boldsymbol{I} & \Delta t \boldsymbol{R}_k^I & -\frac{\Delta t^2}{2}\boldsymbol{R}_k^I \\ \boldsymbol{0} & \boldsymbol{R}_{k+1}^{I\,T}\boldsymbol{R}_k^I & -\Delta t \boldsymbol{R}_{k+1}^{I\,T}\boldsymbol{R}_k^I \\ \boldsymbol{0} & \boldsymbol{0} & \boldsymbol{R}_{k+1}^{I\,T}\boldsymbol{R}_k^I \end{bmatrix} \begin{bmatrix} \boldsymbol{p} \\ {}^B\boldsymbol{v} \\ \boldsymbol{b_a} \end{bmatrix}_k + \begin{bmatrix} \frac{\Delta t^2}{2}\boldsymbol{R}_k^I \\ \Delta t \boldsymbol{R}_{k+1}^{I\,T}\boldsymbol{R}_k^I \\ \boldsymbol{0} \end{bmatrix} \left({}^B\boldsymbol{a}_k - \boldsymbol{R}_k^{I\,T\,I}\bar{\boldsymbol{g}}_k\right) + \begin{bmatrix} \boldsymbol{I} & -\frac{\Delta t^2}{2}\boldsymbol{R}_k^I & \boldsymbol{0} \\ \boldsymbol{0} & -\Delta t \boldsymbol{R}_{k+1}^{I\,T}\boldsymbol{R}_k^I & \boldsymbol{0} \\ \boldsymbol{0} & \boldsymbol{0} & \boldsymbol{R}_{k+1}^{I\,T}\boldsymbol{R}_k^I \end{bmatrix} \begin{bmatrix} \boldsymbol{n_p} \\ \boldsymbol{n_a} \\ \boldsymbol{n_{b_a}} \end{bmatrix}_k \tag{27}$$

$$\boldsymbol{y_{p}}_k = \begin{bmatrix} \boldsymbol{I} & \boldsymbol{0} & \boldsymbol{0} \\ \boldsymbol{0} & \boldsymbol{I} & \boldsymbol{0} \end{bmatrix} \begin{bmatrix} \boldsymbol{p} \\ {}^B\boldsymbol{v} \\ \boldsymbol{b_a} \end{bmatrix}_k + \boldsymbol{\Theta}_k$$

where $\boldsymbol{n_{p}}_k$ is a zero-mean Gaussian white noise that accounts for disturbance in the position. The proposed position observer with acceleration bias, depicted in Fig. 1, is given by the following nonlinear feedback system:

$$\begin{bmatrix} \hat{\boldsymbol{p}} \\ {}^B\hat{\boldsymbol{v}} \\ \hat{\boldsymbol{b}}_{\boldsymbol{a}} \end{bmatrix}_{k+1} = \begin{bmatrix} \boldsymbol{I} & \Delta t \boldsymbol{R}_k^I & -\frac{\Delta t^2}{2}\boldsymbol{R}_k^I \\ \boldsymbol{0} & \boldsymbol{R}_{k+1}^{I\,T}\boldsymbol{R}_k^I & -\Delta t \boldsymbol{R}_{k+1}^{I\,T}\boldsymbol{R}_k^I \\ \boldsymbol{0} & \boldsymbol{0} & \boldsymbol{R}_{k+1}^{I\,T}\boldsymbol{R}_k^I \end{bmatrix} \begin{bmatrix} \hat{\boldsymbol{p}} \\ {}^B\hat{\boldsymbol{v}} \\ \hat{\boldsymbol{b}}_{\boldsymbol{a}} \end{bmatrix}_k + \begin{bmatrix} \frac{\Delta t^2}{2}\boldsymbol{R}_k^I \\ \Delta t \boldsymbol{R}_{k+1}^{I\,T}\boldsymbol{R}_k^I \\ \boldsymbol{0} \end{bmatrix} \left({}^B\boldsymbol{a}_k - \boldsymbol{R}_k^{I\,T\,I}\bar{\boldsymbol{g}}_k\right) + \begin{bmatrix} \boldsymbol{K_{1p}} & \boldsymbol{K_{1v}} \\ \boldsymbol{K_{2p}}\boldsymbol{R}_{k+1}^{I\,T} & \boldsymbol{K_{2v}}\boldsymbol{R}_{k+1}^{I\,T} \\ \boldsymbol{K_{3p}}\boldsymbol{R}_{k+1}^{I\,T} & \boldsymbol{K_{3v}}\boldsymbol{R}_{k+1}^{I\,T} \end{bmatrix} \underbrace{\begin{bmatrix} \boldsymbol{p}_k - \hat{\boldsymbol{p}}_k + \boldsymbol{\Theta}_{1\,k} \\ \boldsymbol{R}_k^I\left({}^B\boldsymbol{v}_k - {}^B\hat{\boldsymbol{v}}_k\right) + \boldsymbol{\Theta}_{2\,k} \end{bmatrix}}_{\boldsymbol{y}_k} \tag{28}$$

where the hat is used to denote an estimate, $\boldsymbol{p}_k$ and ${}^B\boldsymbol{v}_k$ are the observed position and velocity corrupted by a Gaussian zero-mean white-noise $\boldsymbol{\Theta}_k$, and $\boldsymbol{K_{ip}}$ and $\boldsymbol{K_{iv}} \in$ M(3,3) are feedback gain matrices. The position observation $\boldsymbol{p_k}$ can be obtained by vision-based algorithms.

Rewriting the position kinematics (24) considering $\boldsymbol{R}^I = \boldsymbol{I}$ and without input results in the following linear time invariant system:

$$\begin{bmatrix} \boldsymbol{X_p} \\ \boldsymbol{X_{B_v}} \\ \boldsymbol{X_{b_a}} \end{bmatrix}_{k+1} = \begin{bmatrix} \boldsymbol{I} & \Delta t\boldsymbol{I} & -\frac{\Delta t^2}{2}\boldsymbol{I} \\ \boldsymbol{0} & \boldsymbol{I} & -\Delta t\boldsymbol{I} \\ \boldsymbol{0} & \boldsymbol{0} & \boldsymbol{I} \end{bmatrix} \begin{bmatrix} \boldsymbol{X_p} \\ \boldsymbol{X_{B_v}} \\ \boldsymbol{X_{b_a}} \end{bmatrix}_k + \begin{bmatrix} \boldsymbol{I} & -\frac{\Delta t^2}{2}\boldsymbol{I} & \boldsymbol{0} \\ \boldsymbol{0} & -\Delta t\boldsymbol{I} & \boldsymbol{0} \\ \boldsymbol{0} & \boldsymbol{0} & \boldsymbol{I} \end{bmatrix} \begin{bmatrix} \boldsymbol{n_p} \\ \boldsymbol{n_a} \\ \boldsymbol{n_{b_a}} \end{bmatrix}_k \tag{29}$$

Theorem 3. Consider the discrete-time system (27). Let $\boldsymbol{K_{ip}}$ and $\boldsymbol{K_{iv}}$ be the steady-state Kalman gains for the system (29). Then the position complementary filter (28) is uniformly asymptotically stable (UAS).

Proof. The proof is omitted due to its extension. □

Proposition 4. Let the state and observation disturbances in the position kinematics (27) be characterized by the zero-mean Gaussian white noises $\boldsymbol{n_p}$, $\boldsymbol{n_a}$, $\boldsymbol{n_{b_a}}$ and $\boldsymbol{\Theta}_k$, respectively. Then the complementary filter (28) is the "steady state" Kalman filter for the system (27) in the sense that the Kalman feedback gain K_{optk} converges asymptotically as follows:

$$\lim_{k\to\infty} \left\| \boldsymbol{K_{opt}}_k - \begin{bmatrix} \boldsymbol{K_{1p}} & \boldsymbol{K_{1v}} \\ \boldsymbol{K_{2p}}\boldsymbol{R}_{k+1}^{I\,T} & \boldsymbol{K_{2v}}\boldsymbol{R}_{k+1}^{I\,T} \\ \boldsymbol{K_{3p}}\boldsymbol{R}_{k+1}^{I\,T} & \boldsymbol{K_{3v}}\boldsymbol{R}_{k+1}^{I\,T} \end{bmatrix} \right\| = \boldsymbol{0} \tag{30}$$

Proof. An analogous proof can be found in theorem 4 of Vasconcelos et al. (2011).

3. NAVIGATION SYSTEM IMPLEMENTATION

This section presents the overall navigation system architectures designed by the combination of the attitude filter (2.1) with the two position filters proposed in Section 2 and described by (21) and (28). All the measurement vectors are discussed including the employed vision algorithms for pose measurements and sampling rates exploited.

3.1 Observations

Camera tracking system. The measurement of the position filters (21) and (28) are given by a landmark localization system consisting of 6 markers. The landmarks are dispersed in a coplanar way. A YCbCr color segmentation via Mahalanobis distance was used to segment the markers from the background. The choice of such distance is due to its scale-invariant property and since it takes into account not only the mean but also the covariance between color data, it does not ignore uncertainties. According to Gonzalez and Woods (2002), the Mahalanobis distance is given by:

$$\boldsymbol{D}(\boldsymbol{z},\boldsymbol{\mu}) = \sqrt{(\boldsymbol{z}-\boldsymbol{\mu})^T\boldsymbol{C}^{-1}(\boldsymbol{z}-\boldsymbol{\mu})} \tag{31}$$

where $\boldsymbol{C}$ is the estimated covariance matrix of the marker's C_b and C_r color components, $\boldsymbol{\mu}$ is the estimate average and $\boldsymbol{z}$ represents the observed vector values of C_b and C_r.

By applying this method it is possible to segment some specific color from an image in an efficient and effective way by performing the following statistical test:

$$\boldsymbol{D}(\boldsymbol{z},\boldsymbol{\mu})^2 \leq \gamma \tag{32}$$

where gamma is the threshold that represents the correct associations allowed to be acceptable.

After segmenting the markers their centroid is computed and the PnP problem arises. The RPnP solution, from Li et al. (2012), was chosen since it is faster and less prone to noise than the traditional Direct Linear Transform (DLT) solution for the number of used points (Zheng et al. (2013)). The solution provides the position and orientation of the camera relative to the landmarks plane. Only the position in X, Y-axis and the yaw angle was used as a measurement.

With the interest of optimizing the tracking of the marker different algorithms were proposed. The most important was adding recursion to the system such that every time the reprojection error of the previous step is less than the desired threshold the image point position (u,v) is sent to the next step, making the tracking more accurate by increasing the threshold γ in these areas. Another advantage is that there is no need of computing the Mahalanobis distance (31) in the whole image for each step.

Unlike the DevKit platform, the Target platform, has access to the full image resolution with no additional delay. So an higher resolution image can be used to track the markers whenever the recursive algorithm found them and the total pixel area to be tracked does not exceed the maximum allowed processing power.

The overall camera algorithm flowchart is shown in Fig. 2.

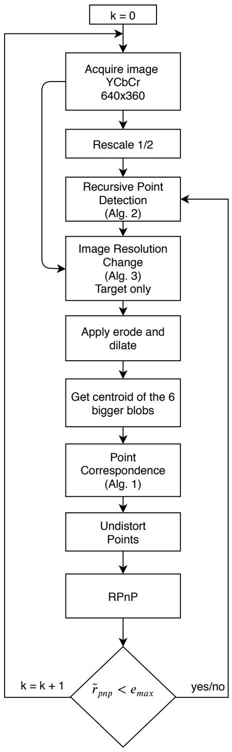

Fig. 2. Vision algorithm flowchart.

Euler angles. The attitude observation $\boldsymbol{\lambda}_k$ in Euler angles is determined by the Earth's gravitational field and by the camera tracking system. The pitch and roll angles are obtained from the compensated accelerometer measurements by the centripetal acceleration or by the estimated acceleration bias from the second position filter. Depending on the architecture used the acceleration is estimated as:

$$Architecture\ 1:\ \hat{\boldsymbol{g}} = \boldsymbol{a_c} - \boldsymbol{\omega} \times ({}^B\boldsymbol{v} - \hat{\boldsymbol{b}}_v) \tag{33a}$$

$$\begin{aligned} Architecture\ 2:\ \hat{\boldsymbol{g}} &= \boldsymbol{a_c} - (\boldsymbol{a_c} - \boldsymbol{R}_k^{I\,T}\boldsymbol{g} - \hat{\boldsymbol{b}}_{\boldsymbol{a}}) \\ &= \boldsymbol{R}_k^{I\,T}\boldsymbol{g} + \hat{\boldsymbol{b}}_{\boldsymbol{a}} \end{aligned} \tag{33b}$$

For the architecture 1, a low pass filter with a cut off frequency of 10Hz is applied to cut high frequency dynamics before computing roll and pitch as follows:

$$\begin{aligned} \phi &= -atan_2\left(\hat{g}_y, -\hat{g}_z\right) \\ \theta &= -atan_2\left(-\hat{g}_x, \sqrt{\hat{g}_y^2 + \hat{g}_z^2}\right) \end{aligned} \tag{34}$$

For the architecture 2, the lowpass is not employed since the high frequency dynamics, linear and centripetal accelerations, are estimated from the position filter and removed from the accelerometer raw.

The yaw observation ψ can be given by the camera tracking algorithm or by the magnetometer vector. For the Target platform both measurements are used and filtered before entering in the attitude filter with a simple KF. The yaw angle ψ from the calibrated magnetometer vector is retrieved as:

$$\psi_{mag} = -atan_2\left(m_{cy}c_\phi - m_{cz}s_\phi, m_{cx}c_\theta + m_{cy}s_\phi s_\theta + m_{cz}c_\phi s_\theta\right) \tag{35}$$

3.2 Filter coupling

The global filter architectures is depicted in Fig. (3). The proposed navigation systems are composed by coupling the attitude with one of the two position filters proposed. For both architectures, the attitude terms $\boldsymbol{R}_k^I$ and $\boldsymbol{Q(\lambda}_k)$ are obtained using the last available estimate of the attitude filter $\hat{\boldsymbol{\lambda}}$, since it is the best estimation available. The yaw angle measurement given by the camera algorithm has a frequency of 20Hz. If the magnetometer is not used, since the attitude filter works at 100Hz, whenever a measurement is not available the yaw estimate will depend on gyroscope only. To workaround the optimality of a multi-rate system see Bittanti et al. (1991). In case of ψ_{mag} being available, a pre-filter estimates ψ and a bias b_ψ by considering the yaw measurements ψ_{cam} and ψ_{mag}, where ψ_{mag} is assumed to have a time-varying bias.

Architecture 1 The compensated body linear and angular velocities are used to estimate the centripetal acceleration, making it possible to remove angular acceleration from the accelerometer measurements.

Architecture 2 The body acceleration bias $\boldsymbol{b_a}$ to compensate the accelerometer for linear and centripetal accelerations. The position filter (28) adopted a new attitude update kinematic term $\boldsymbol{R}_{k+1}^{I\,T}\boldsymbol{R}_k^I \approx e^{\Delta t\left(\omega_{rk} - \hat{\boldsymbol{b}}_{\boldsymbol{\omega}k}\right)_\times}$, which is obtained using the compensated angular velocities. $(\boldsymbol{a})_\times$ denotes the skew matrix of the vector $\boldsymbol{a} \in \mathbb{R}^3$.

The theoretical stability and performance properties of the filters derived and explained in Section **??** cannot be fulfilled for the entire architecture 1 due to filter coupling and the use of pendular measurements in the attitude observation filter. If the roll and pitch measurements from the vision-based observation were used it could be guaranteed. To get those measurements, an higher rate and resolution is required in the segmentation algorithm to get faster and less noisy attitude observations at the cost of higher computational cost. Another solution would be to use more markers. In architecture 2, the accelerometer is compensated for the linear and centripetal accelerations. It follows that architecture 2 will not suffer from pendular measurements issues as in architecture 1. However, the coupling issues are still present.

4. EXPERIMENTAL RESULTS

4.1 Ar Drone 2.0 UAV

The data acquisition and telemetry processes were carried out in the Parrot AR.Drone 2.0 shown in Fig. (4). This UAV is a low-cost quadcopter available in the commercial market. Parrot has also released a Software Developing Kit (SDK), to enable developers to produce their own application. This work exploits two different built-in Simulink platforms available online to communicate with the vehicle, the AR.Drone Simulink Development-Kit V1.1 (DevKit) from Sanabria (2014) and AR.Drone 2.0 Quadcopter Embedded Coder from Sanabria (2014).

The DevKit platform was modified to be able to access sensor data at 100Hz. The inner control loop processes used are the factory ones and it runs onboard. The outer loop is controlled via Wi-Fi and has limitations in terms of given references. This platform allows the use of the factory OF's velocity as an input in the first position filter (21), as a measurement in the second position filter.

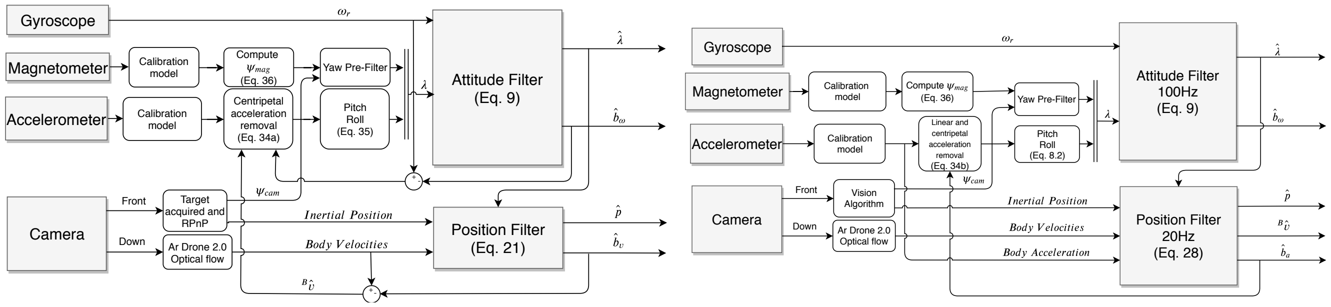

Fig. 3. Global filter architectures, 1 at left and 2 at right.

To get access to the front camera in the DevKit *Simulink* platform, a *C++* open source project, *CVDrone* from Shinpuku (2017), was used to decode the factory video stream with the help of *OpenCV* and then to send it via UDP host to *Simulink* in JPEG format. The observed delay is similar to the one experienced by the DevKit platform, around 250ms, so there were not any additional problems. The yaw pre-filter has not been used here due to problems on the access to the magnetometer in the DevKit platform.

All of the implementations were ran on the host computer that is connected to the drone via Wi-Fi. The UAV receives input controls of roll and pitch angles, yaw rate and vertical velocities and retrieves a packet with all data sensors and estimations of horizontal velocities, Euler angles and height.

All the code was tested and ran in real time onboard of the UAV using the second platform, which is a Target solution that provides full access to the hardware, allowing for the replacement of the inner control processes and for the full software to run on the UAV processor. Due to the unavailability of an optic flow algorithm on this platform external cameras were used to estimate horizontal velocities.

Thus, since the DevKit merely relies on onboard sensors, the presented results here were achieved through this platform. For this experiment, the only data used from the DevKit received packet was the gyroscope raw, accelerometer raw, OF velocities and front camera video stream.

4.2 Parameter Design

The complementary frequency response of the closed loop by considering $\boldsymbol{I}$ in place of $\boldsymbol{Q}(\boldsymbol{\lambda}_k)$ and $\boldsymbol{R}_k^I = \boldsymbol{I}$ was used for filter design, using the systems (9), (21) and (27). As discussed in Subsection 2.1, the proposed position filters are identified with the steady-state Kalman filter and the attitude filter for constant pitch and roll angles.

All the following results were captured in real time using the architecture 2 to control the vehicle with the parameters of Table 1. To compare the estimates with the results of architecture 1, offline computation, with flight data, were performed using architecture 1 with the parameters shown in Table 1 as well and its RMSE values computed for comparison, see Table 3.

A constant sampling rate of 20Hz was used for both front camera and position filter systems with a resolution of 320×180 pixels. The attitude filter worked at 100Hz. The adopted weights, respective gains and gyroscope correlation times $\boldsymbol{T}$ are detailed in Table 1. The attitude process noise matrix was designed based on the AV noise covariance from the gyroscope as explained in Section 2.1 and on the gyroscope variance when the fans were active. The attitude observation weights were designed in order for the filter to react well in both low dynamics and not to drift too much when high dynamics are demand.

The position process noise matrix was adjusted based on the maximum variations that the state variables change with time. A value close to zero means that the state only slight varies with time. The position observation noise matrix was modeled based on the measurement variance and reliability.

As shown in Fig. 5, the low-frequency region of the observation angles and camera position measurement are blended with the high-frequency contents of the open-loop integration of the inertial measurements and OF velocity.

4.3 Analysis

The experiments were made indoor and in order to assess the estimates, a precision set of cameras (Qualisys Motion Tracking) was used as ground truth validation. The characteristics of the tracking system are listed in Table 2. Only the X and Y axis of position is analyzed.

Cameras	Qualisys Pro Reflex 1000
Frequency	$<$ 200Hz
Markers	19mm markers
Precision	<1mm and <0.2° after calibration

Table 2. Qualisys Tracking System properties.

All data is compared against the ground truth (Qualisys) in the landmarks inertial frame. Every time the UAV could not segment the six markers properly, the position filter relies only on the OF and the attitude filter relies only on the Z-axis gyro to estimate yaw. Those times are depicted with green circles in the results. Areas with a large portion of no observation are depicted with a gray background.

The position results are coherent with the ground truth, as evidenced in Fig. 6. The best estimation is in X-axis (perpendicular to the landmark's plane) due to the slightly less noisy position observation, Fig. 6(a-b) see histograms. The maximum error in X and Y, while measurements were available, were no more than 7 and 10cm, respectively, except between [80-110]sec where the camera tracking system failed especially in Y, due to high yaw values (see Fig. 9-yaw), and high distance from the target (around

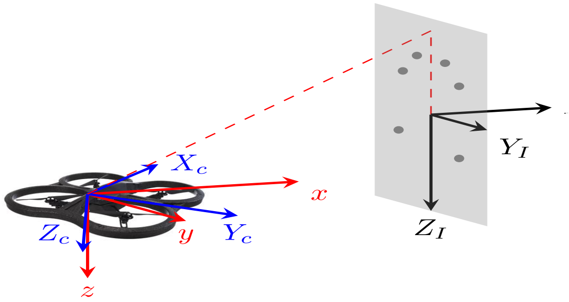

Fig. 4. Parrot Ar Drone 2.0 with camera and Inertial frames.

Filter	State Weights	Observation Weights
Attitude (100Hz)	$\boldsymbol{Q_{\lambda}} = \mathrm{diag}(8,5,8)$ $\boldsymbol{Q_{b_{\omega 1}}} = \mathrm{diag}(1.6, 2.9, 0.5) \times 10^{-6}$ $\boldsymbol{Q_{b_{\omega 2}}} = \mathrm{diag}(25, 25, 0.5) \times 10^{-10}$	$\boldsymbol{R_{\lambda}^{a1}} = \mathrm{diag}(5,5,5) \times 10^{2}$ $\boldsymbol{R_{\lambda}^{a2}} = \mathrm{diag}(12.5, 25, 250) \times 10^{2}$ Model Parameters: $\boldsymbol{T} = \mathrm{diag}\left(\frac{1}{10}, \frac{1}{15}, \frac{1}{100}\right)$
Position A1 (20Hz)	$\boldsymbol{Q_{p}} = \mathrm{diag}(0.1, 0.1)$ $\boldsymbol{Q_{b_v}} = \mathrm{diag}(1,1) \times 10^{-5}$	$\boldsymbol{R_{p}} = \mathrm{diag}(0.05, 0.1, 0.05)$
Position A2 (20Hz)	$\boldsymbol{Q_{p}} = \mathrm{diag}(5,5,5) \times 10^{-4}$ $\boldsymbol{Q_{v}} = \mathrm{diag}(1,1,1)$ $\boldsymbol{Q_{b_a}} = \mathrm{diag}(1,1,1) \times 10^{-3}$	$\boldsymbol{R_{p}} = \mathrm{diag}(0.1, 0.1, 0.00001)$ $\boldsymbol{R_{v}} = \mathrm{diag}(0.05, 0.05, 0.05)$

Table 1. Complementary Filters Parameters.

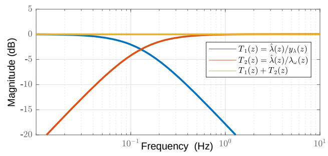

(a) Attitude filter.

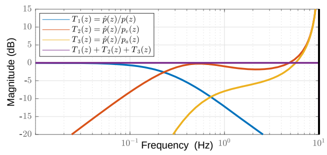

(b) Position filter 2.

Fig. 5. Filters Bode diagrams - A2 DevKit

3m), producing a noisy and biased observation. The root-mean-square-error (RMSE) of the position, considering that observations are available, is detailed in Table 3.

The heavy drift [140-150]sec was caused due to high accelerations while no observation was available. These high dynamics caused poor OF velocity estimates (see Fig. 7), that were integrated and not compensated. Nevertheless, the filter rapidly converged right after the observation was available, see position error in Fig. 6(a-b).

The linear velocity estimates versus the ground-truth are shown in Fig. 7. The proposed filter estimates the linear velocity explicitly. The error shown goes above 0.4m/s which is not entirely true. Due to the fact that imperfect estimate and ground truth alignment at the time of error is being computed, a misleading error result occurs for high signals variations. The overall velocity RMSE is shown in Table 3.

The acceleration bias and the body gravitational vector estimates are depicted in Fig. 8. It is clear to see the resemblance between the ground truth and the estimates. The attitude estimation results are consistent with the ground truth. The yaw estimate error was no more than 4 degrees, with a RMSE of 1.24 degrees, while observation was available (see Fig. 9(b)). The maximum error, 4.8 degrees, occurred at 147sec due to lack of observation and drift from the gyroscope. The yaw estimate can be seen slowly converging to the observation right after measurement becomes available.

Compared with the ground truth, the pitch and roll angles followed well the ground truth resulting in a maximum error no more than 2 degrees, respectively, depicted in Fig. 9(a-b). The RMSE of attitude, considering that observations are available, is detailed in Table 3. A statistical representation of the errors in the UAV orientation can be seen in Fig. 9(c-d-e).

The angular velocity estimation is shown in Fig. 10. The proposed filter does not estimate the angular velocity explicitly, but it compensates with two bias terms. This estimate is given by the gyroscope raw and by the bias estimate which is depicted in Fig. 10.

The experimental results obtained onboard the Ar Drone 2.0 validate the proposed INS. The adopted design parameters yield the desired sensor fusion in the frequency domain accomplishing good attitude and position estimation. The attitude and position estimates were consistent with the given trajectory, and the INS endured landmark outage for small dynamics, which shows that the proposed complementary filter based architecture is suitable for GPS denied applications.

5. CONCLUSION

In this work, two INSs based on complementary filters that rely on inertial and vision sensors were presented. The existence of a varying gyroscope bias based on AV was considered and its value estimated by the observer. The vision algorithm was shown to be computationally efficient and able to run in real time onboard of the vehicle with the implemented filters and controllers. Two different INS were implemented, the first with the attitude filter and the position filter with velocity bias, and the second with the same attitude filter but with a position filter that estimates linear acceleration bias. The second architecture proved to achieve similar results of position and better of attitude when compared with architecture 1.

ACKNOWLEDGEMENTS

This work was supported by FCT, through IDMEC, under LAETA, project UID/EMS/50022/2019.

REFERENCES

Anderson, B. and Moore, J. (1979). *Optimal Filtering*. Prentice-Hall, Englewood Cliffs, NJ.

Bittanti, S., Colaneri, P., and De Nicolao, G. (1991). *The Periodic Riccati Equation*, 127–162. Springer Berlin Heidelberg, Berlin, Heidelberg.

Crassidis, J.L., Markley, F.L., and Cheng, Y. (2007). A survey of nonlinear attitude estimation methods. *Journal of Guidance, Control, and Dynamics*, 30, 12–28.

Gelb, A. (1974). *Applied Optimal Estimation*. The MIT Press.

Gonzalez, R.C. and Woods, R.E. (2002). *Digital Image Processing*. Prentice Hall, 2 edition.

Jazwinski, A.H. (1970). *Stochastic processes and filtering theory*. Number 64 in Mathematics in science and engineering. Acad. Press, New York, NY [u.a.].

Arch.	X(cm)	Y(cm)	Z(cm)	Vx(cm/s)	Vy(cm/s)	Vz(cm/s)	yaw(°)	pitch(°)	roll(°)
1	3.4	7.9	1.2	5.9	4.3	4.2	1.22	0.79	0.76
2	3.3	7.6	1.1	6.0	4.2	4.0	1.14	0.59	0.47

Table 3. Experimental RMSE, observation available - Arch. 1 and Arch. 2 comparison DevKit

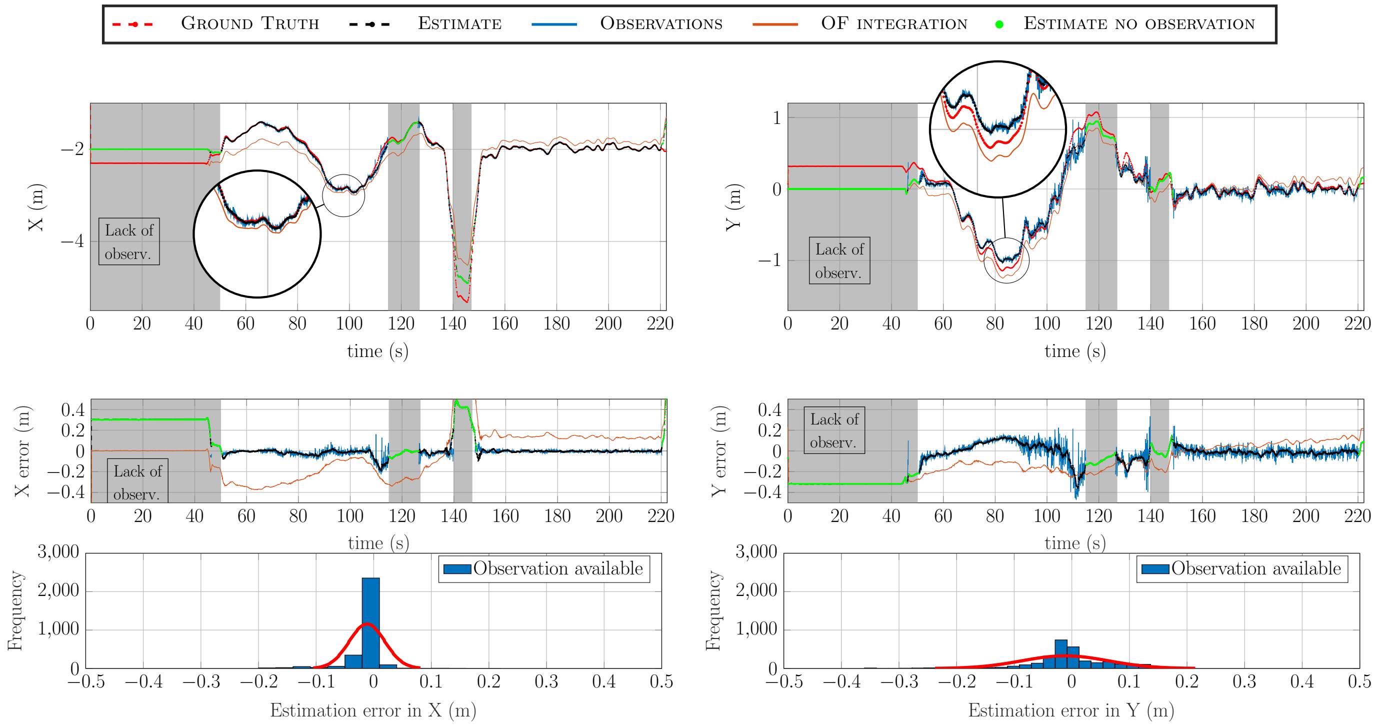

(a) X-axis (b) Y-axis

Fig. 6. Trajectory estimation results in X and Y axis.

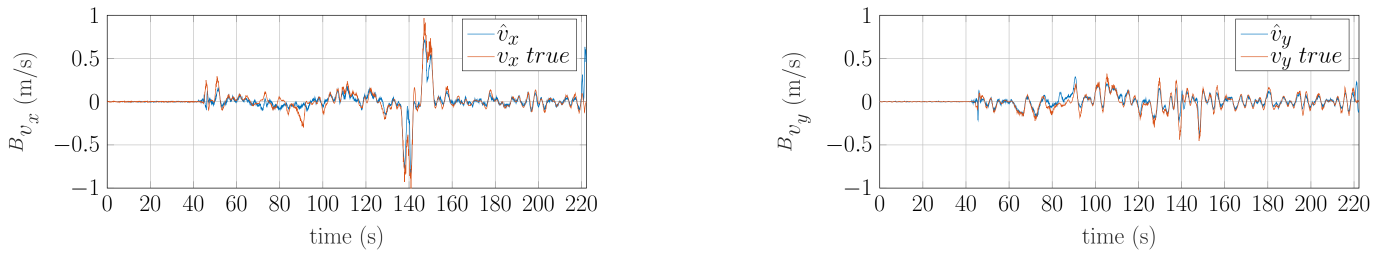

Fig. 7. Body linear velocities - Arch. 2 DevKit

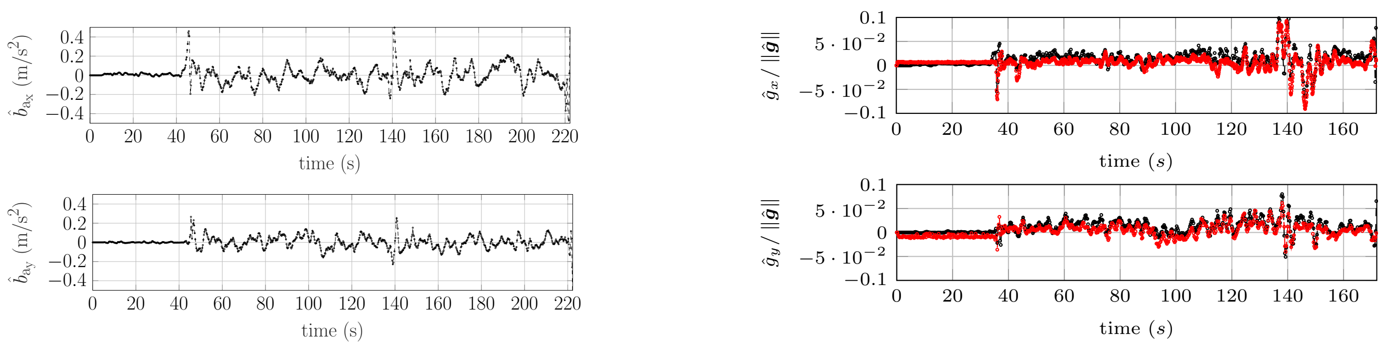

Fig. 8. Body linear and centripetal acceleration biases (left) and estimate of the body normalized gravitational vector (right) - Arch. 2 DevKit

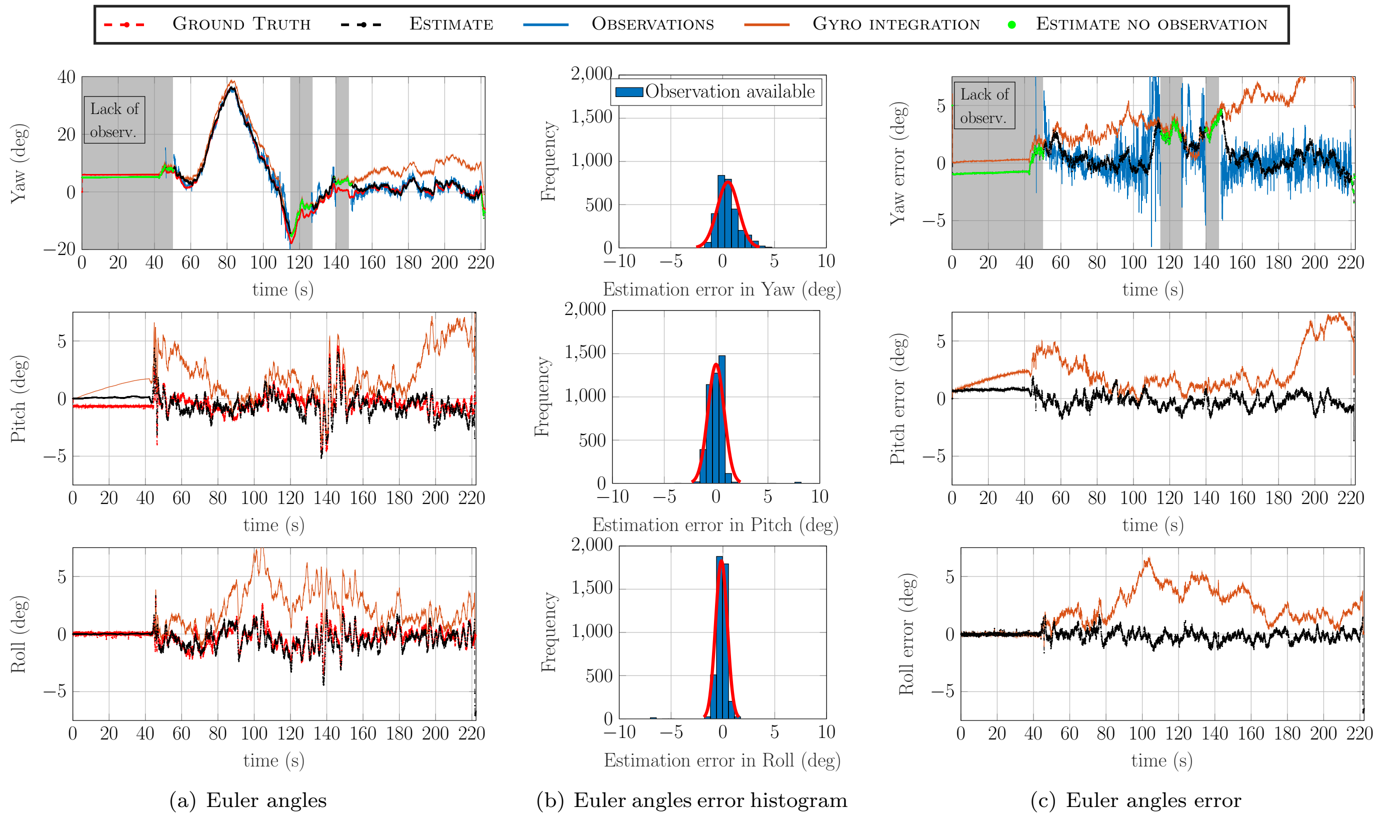

Fig. 9. Attitude estimation results.

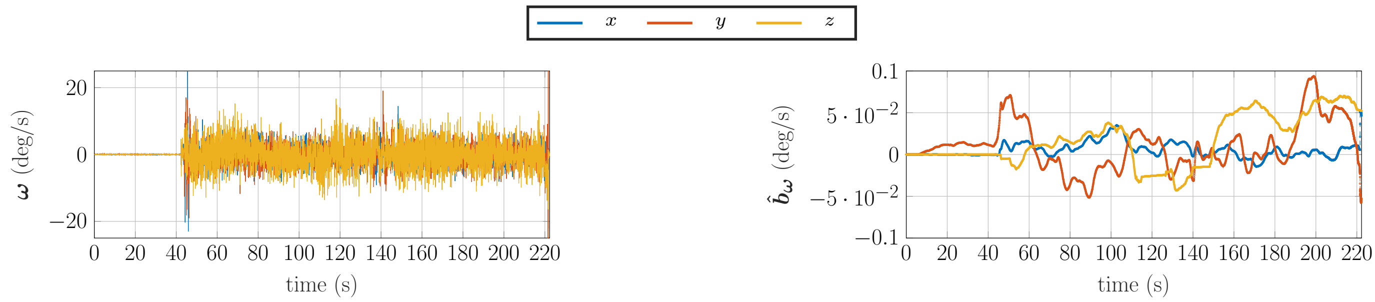

Fig. 10. Body angular velocities and respective bias estimation.

Li, S., Xu, C., and Xie, M. (2012). A robust o(n) solution to the perspective-n-point problem. *IEEE Transactions on Pattern Analysis and Machine Intelligence*, 34, 1444–1450.

Mahony, R., Hamel, T., and Pflimlin, J. (2008). Nonlinear complementary filters on the special orthogonal group. *IEEE Transactions on Automatic Control*, 53(5), 1203–1218.

Maybeck, P.S. (1994). *Stochastic Models, Estimation, and Control*. Academic Press.

Mohamed, N., Al-Jaroodi, J., Jawhar, I., Idries, A., and Mohammed, F. (2018). Unmanned aerial vehicles applications in future smart cities. *Technological Forecasting and Social Change*.

Ünver, A. (2013). *Determination of Stochastic Model Parameters of Inertial Sensors*. Ph.D. thesis, Middle East Technical University, Electric Electronic Engineering Department.

P. Crain, T., Bishop, R., and Brady, T. (2010). Shifting the inertial navigation paradigm with mems technology.

Petkov, P. and Slavov, T. (2010). Stochastic modeling of mems inertial sensors. *Cybernetics and Information Technologies*, 10.

Quinchia, A.G., Falco, G., Falletti, E., Dovis, F., and Ferrer, C. (2013). A comparison between different error modeling of MEMS applied to GPS/INS integrated systems. *Sensors (Switzerland)*, 13(8), 9549–9588.

Rugh, W.J. (1996). *Linear system theory*. Prentice Hall,, Upper Saddle River, N.J., 2nd ed. edition.

Sanabria, D.E. (2014). Ar drone simulink development-kit v1.1. https://www.mathworks.com/matlabcentral/fileexchange/43719-ar-drone-simulink-development-kit-v1-1.

Shinpuku, N. (2017). Cv drone project. https://github.com /puku0x/cvdrone.

Vasconcelos, J.F., Cardeira, B., Silvestre, C., Oliveira, P., and Batista, P. (2011). Discrete-time complementary filters for attitude and position estimation: Design, analysis and experimental validation. *IEEE Transactions on Control Systems Technology*, 19(1), 181–198.

Zheng, Y., Kuang, Y., Sugimoto, S., Åström, K., and Okutomi, M. (2013). Revisiting the pnp problem: A fast, general and optimal solution. In *2013 IEEE International Conference on Computer Vision*, 2344–2351.